# DISCRIMINATION OF WATER AND ICE CLOUD USING ALBEDO DIFFERENCE OF MULTIPLE VISIBLE BAND OF HIMAWARI-8 DATA

Destri Yanti Hutapea (1), Babag Purbantoro (1)

[1] Remote Sensing Technology and Data Center, Indonesian Institute of Aeronautics and Space (LAPAN), Jakarta, Indonesia
Email: destri.yanti@lapan.go.id; babag.purbantoro@lapan.go.id

**KEYWORDS:** ice cloud, water cloud, albedo difference, Himawari-8

**ABSTRACT:** Cloud detection and classification form a fundamental knowledge in weather analysis. Mostly, clouds are divided into two, water cloud and ice cloud, based on constituent particles. The water particle is the substance in the atmosphere that is grouping as a liquid (water cloud), and solid (ice cloud). Albedo is one of the variables used for discriminating water and ice clouds from remote sensing satellite imagery reflectance. This algorithm has been studied as the simplest way to detect and identify water and ice clouds in the atmosphere using satellite data. Owing to its high temporal resolution, the recent availability of Himawari-8 Advanced Himawari Imager (AHI) has enhanced the possibility of better rapid water/ice cloud classification. The technique is to exploit the use of albedo difference values using multiple visible bands of AHI. In this study, we apply the albedo difference between 1.6μm and 2.3μm bands. We implement the analysis using ten datasets in the summer and winter season located around Japan in the daytime only (02.00 – 05.00 UTC). The verification of the accuracy was done by using space-borne Lidars, namely, Cloud-Aerosol Lidar and Infrared Pathfinder Satellite Observation (Calipso) data, and ground temperature measurement data. The depolarization ratio of Calipso data was used for identifying the cloud phase. The cloud altitude was verified by ground measurement data. We decided and picked the time and location based on the Calipso data availability. The result of verification showed that the accuracy of the cloud mask was averaged around 86% (73% for cloud phase) and 89% (73%) in the summer and winter season respectively.

## 1. INTRODUCTION

The cloud phases are highly influenced by their growth, diverging the clouds of water and ice. In the radiation budget, water and ice are absorbed weakly in the near-infrared radiation. Besides, in the region of 1.55 and 1.75 μm, their spectral absorption differs (Twomey and Cocks, 1982). It is noted that clouds forming at temperatures warmer than 0°C contain only liquid droplets (spherical), whereas those occurring at temperatures colder than -40°C normally consist solely of ice crystals (non-spherical) (Hu *et al.*, 2003). Cloud optical thickness is largely influencing the reflectance in non-absorbing channels (0.67-1.2μm), while longer-wavelength absorbing near-infrared bands (1.6-3.7μm) provide the cloud particle size information. The difference of reflectance in the near-infrared bands differs from the water and ice cloud that has a different size of the constituent particle. This algorithm has been studied as a simple way to detect and identify water and ice clouds (Scorer, 1989)(Hu *et al.*, 2003). Simple cloud detection also has been done using 0.47μm of Himawari-8 and MODIS reflectance during the daytime (Purbantoro *et al.*, 2019a)(Platnick *et al.*, 2001). Due to the need for rapid cloud monitoring analysis, the processing system needs a simple technique to speed up the processing. Threshold-based is considered as a simple cloud detection and classification technique (Inoue and Ackerman, 2002)(Lutz *et al.*, 2003), but also takes into account its performance accuracy (Purbantoro *et al.*, 2019b). Recently, the cloud phase detection was done by using the threshold and ratio of the near-infrared and visible band (Chylek *et al.*, 2006).

The Himawari-8 was launched and fully operated by the Japan Meteorological Agency (JMA) in May 2015. Advanced Himawari Imager (AHI) sensor onboard the Himawari-8 meteorological satellite sensor has enabled a very high-frequency cloud observation. It has a 10 minutes temporal resolution for full-disk data and provides 16 bands including visible, near-infrared, and thermal infrared spectral regions (Bessho *et al.*, 2016). Based on this advantage, Himawari-8 is considered as the main data for a rapid cloud monitoring system. The Cloud-Aerosol Lidar and Infrared Pathfinder Satellite Observations (Calipso) satellite were operated In April 2006, to deliver worldwide vertically established cloud and aerosol measurements to distinguish clouds consisting of both ice and liquid that are not easily detected by conventional passive sensors (Hu *et al.*, 2009).

In the present study, we exploit the use of albedo difference values using multiple visible bands of AHI between 1.6μm and 2.3μm spectral bands to differentiate the water and ice cloud. The verification of the accuracy was done by the depolarization ratio of Calipso data in both cloud detection and phase detection. A similar technique of using Calipso data has been reported by the previous study (Kay *et al.*, 2016). We also determine the cloud altitude and verify it using ground measurement data and lapse rate method. The validation is checking the cloud altitude whether as low cloud (dominated by water cloud, lower than 3 km) or high cloud (ice cloud, higher than 6 km).

## 2. METHOD

The datasets location of this study is Japan area which is bounded in 22.02˚N - 47.74˚N and 120.11˚E - 156.99˚E from geo-corrected full disk data of Himawari-8. The Himawari-8 datasets are downloaded from the archive of the Indonesian Institute of Aeronautics and Space (LAPAN). Table 1 shows the datasets obtained when the Calipso satellite overpass the Himawari-8 satellite over Japan area at 02.00-05.00 UTC (11.00-14.00 Japan standard time). To verify the results of the study, we use the CALIPSO data obtained from the NASA Langley Research Center (https:/www-CALIPSO.larc.nasa.gov/). The Calipso data parameters used for this research are the depolarization ratio of the ice/water phase and type of cloud.

Table 1. Date and time of AHI and Calipso datasets.

| #Dataset | Date | AHI | Calipso | Season |
|---|---|---|---|---|
| 1 | July 10, 2019 | 04.00 UTC | 03.58-04.11 UTC | Summer |
| 2 | July 15, 2019 | 03.50 UTC | 03.50-04.04 UTC | Summer |
| 3 | July 17, 2019 | 03.30 UTC | 03.28-03.41 UTC | Summer |
| 4 | August 3, 2019 | 04.20 UTC | 04.21-04.35 UTC | Summer |
| 5 | August 5, 2019 | 04.00 UTC | 03.58-04.12 UTC | Summer |
| 6 | January 12, 2020 | 03.30 UTC | 03.24-03.36 UTC | Winter |
| 7 | January 19, 2020 | 03.00 UTC | 02.55-03.06 UTC | Winter |
| 8 | January 30, 2020 | 03.20 UTC | 03.18-03.30 UTC | Winter |
| 9 | February 13, 2020 | 04.00 UTC | 03.58-04.10 UTC | Winter |
| 10 | February 19, 2020 | 04.30 UTC | 04.16-04.29 UTC | Winter |

### 2.1 Cloud and Phase Detection

For cloud detection, the albedo value for band 1 (0.47μm) of AHI data was determined. Band 1 tends to produce the brightest cloud colors in comparison to other bands. The following formula is used to measure Albedo (*A*) (Japan Meteorological Agency, 2015).

$$I = Gain * Count + Constant, \quad A = c` I . \tag{1}$$

where *I*: radiance; *c'*: transformation coefficient. Then, by multiplying the radiance with the transformation coefficient *c*', a value of *A* is obtained. To get the value of *Gain*, *Constant*, and *c'*, we use the header file of AHI. Cloud object is detected while the value of *A* more than 0.12.

For cloud phase detection, we calculate the albedo of band 5 (1.6μm) dan band 6 (2.3μm) of AHI. The albedo difference between band 5 and band 6 is obtained by subtracting the pixel value from band 5 with a pixel band value of 6. As a result of this subtraction, if the value is lower than zero, it is classified as an ice cloud.

### 2.2 Cloud Mask and Phase Verification

The cloud mask and phase verification were done using Calipso data with the depolarization ratio parameter ($\rho$) (Hu *et al.*, 2009)(Hu, 2007). This verification process is performed by calculating the hit ratio between the cloud detection results and the cloud phase obtained from the $\rho$ value. The cloud detection is indicated by $\rho$ value more than zero. The $\rho$ value below 0.1 and above 0.3 are classified as water cloud and ice cloud respectively (Hu, 2007)(Hu *et al.*, 2003). While $\rho$ value between them is classified as a mix of water and ice cloud. Usually, the later type forms as a low cloud/cumulus and typhoon, that are dominated by the water cloud. The formula used for the hit ratio is adjusted from the previous study as follows (Purbantoro *et al.*, 2019a):

$$Hit\ ratio = \frac{\sum_{i=1}^{n} P_i}{n}, \tag{2}$$

where *Pi* is a constant value derived from

$$P_i = \begin{cases} 1, & \rho \leq 0 \text{ and phase=\{clear area\};} \\ & 0<\rho \leq 0.1 \text{ and phase=\{water cloud\};} \\ & 0.1<\rho \leq 0.3 \text{ and phase=\{mixed that usually dominated by water cloud\};} \\ & \rho \geq 0.3 \text{ and phase=\{ice cloud\}.} \\ 0, & \text{Otherwise.} \end{cases} \tag{3}$$

and *n* is the total number of verified points.

### 2.3 Cloud Altitude Verification

The cloud altitude verification is done by determining the cloud top temperature (CTT) that are represented as brightness temperature (BT) of AHI's band 13. In the atmospheric window spectral band, the CTT tends to be transparent or almost without absorption. We assume that the average lapse rate ($\delta$) in the atmosphere is conditioned around 6.5K/km (Hummel and Kuhn, 1981). Thus, the cloud altitude (*H*) is calculated by using the lapse rate formula (Wengang *et al.*, 2010)

$$H = \frac{1}{\delta}\,(T_s - T_{CT}), \tag{4}$$

where $T_S$ is the surface temperature of the checking point, and $T_{CT}$ is assumed as the CTT value of the 12μm spectral band (AHI's band 13). The checking point is the Tokyo area. The CTT value is a BT of AHIS's band 13 that calculated using the formula as follow,

$$BT = c_0 + c_1 T_e + c_2 {T_e}^2, \tag{5}$$

while

$$T_e = \frac{hc}{k\lambda}\left[\ln\left(\frac{2hc^2}{\lambda^5 I} + 1\right)\right]^{-1}. \tag{6}$$

Here *h* refers to the Planck constant. *k* refers to the Boltzmann constant. *c* refers to the speed of light. $T_e$ is effective temperature, while $c_0$, $c_1$, and $c_2$ are a constant obtained from the Himawari-8 header file.

## 3. RESULTS AND DISCUSSIONS

The albedos of all datasets are calculated using Eq.1. Figure 1(a) shows one of the results of albedo calculation using AHI's dataset #1. The brighter color corresponds to the cloud. We examined that band 1 of AHI delivers the best capability for cloud detection using this method compared with other visible bands. The cloud object is indicated as a higher reflecting color and highly contras with other objects. However, the snow region also has a resemblance with the albedo value as a water cloud as the main error detection. Another error detection is the very thin cloud (very thin cirrus) that usually too transparent for the current method since it is detected as a clear area. Figure 1(b) shows the cloud mask from the cloud detection process. Generally, the result of cloud detection is acceptable and reasonable. However, in the winter season, the snow area is detected as a cloud, while the Calipso recognizes it as a clear area. This error detection reduces the hit ratio of cloud detection and cumulatively reduce the hit ratio of cloud phase detection.

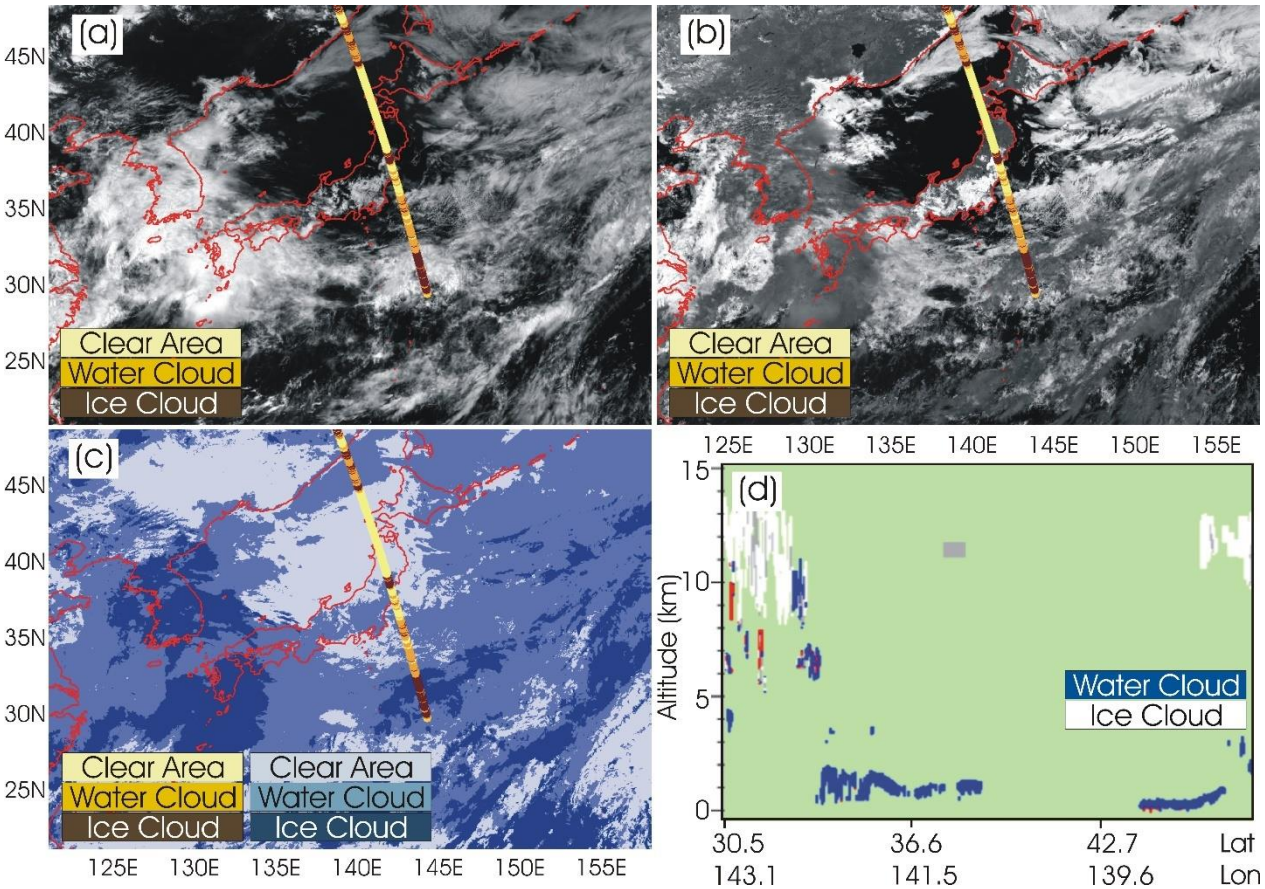


Figure 1. The albedo of AHI's (a) band 1 and (b) band 5. (c) The cloud mask of water and ice cloud. All images are using dataset #1. The brighter color corresponds to the cloud on both images (a and b). The straight line is a Calipso data path that corresponds to the depolarization ratio ($\rho$) value. Yellow, light brown and dark brown correspond to $\rho < 0$, $0 < \rho < 0.3$, and $\rho > 0.3$ respectively. (d) Calipso data altitude time image. The white and blue colors represent the ice and water cloud respectively.

Figure 1(c) shows the result of cloud phase detection based on the albedo difference of band 5 and band 6. As shown in Fig.1(b), it shows that the ice cloud has a darker color than the water cloud in the 1.6μm spectral band. The smaller size of the ice particle has bigger absorption in the atmosphere than the water cloud. The subtraction of band 5 and band 6 is resulting in the negative value as an ice cloud. The ice cloud is mostly dominated by the cirrus cloud in the high altitude (higher than 6km) as shown in Fig. 1(d). It shows the altitude-time image of Calipso data on its path. Generally, the Calipso verification showing a good achievement since there is an acceptable matching between our calculation and Calipso data.

Table 2. The cloud mask and phase hit ratio (column #2-3) and altitude verification (column #4-7).

| #Dataset | Cloud mask hit ratio | Cloud phase hit ratio | Surface Temperature ($T_S$) | Cloud top temperature ($T_{CT}$) | Cloud altitude ($H$) | Water/ice cloud |
|---|---|---|---|---|---|---|
| (1) | (2) | (3) | (4) | (5) | (6) | (7) |
| 1 | 93.9% | 77.2% | 297 K | 289 K | 1.2 km | Water cloud |
| 2 | 88.3% | 82.9% | 295 K | 282 K | 2.0 km | Water cloud |
| 3 | 97.0% | 80.4% | 298 K | 251 K | 7.2 km | Ice cloud |
| 4 | 74.9% | 61.0% | 305 K | 302 K | 0.5 km | Clear area |
| 5 | 76.3% | 65.0% | 305 K | 301 K | 0.6 km | Clear area |
| 6 | 90.0% | 72.0% | 283 K | 259 K | 3.7 km | Water cloud |
| 7 | 96.0% | 70.8% | 282 K | 285 K | 0.0 km | Clear area |
| 8 | 95.0% | 79.8% | 290 K | 291 K | 0.0 km | Clear area |
| 9 | 88.0% | 72.6% | 285 K | 290 K | 0.0 km | Clear area |
| 10 | 79.6% | 67.1% | 284 K | 283 K | 0.2 km | Clear area |

Table 2 shows the result of the hit ratio calculation using Eq.2 and Eq.3. It shows a good achievement of cloud detection as averaged on 86% and 89% hit ratio in summer and winter season respectively. The lowest hit ratio of cloud mask is on dataset #4 and #5 since the clouds are mostly dominated by mixed clouds. Because there is a rain band cloud over Japan area in July and August. It leads to lower hit ratio in the summer season. We found that the more homogenous cloud, the bigger the hit ratio value. The cloud phase hit ratio is averaged on 73% in both summer and winter season. The lowest value of the cloud phase hit ratio is on dataset #4 and #5. The misclassification of water or ice cloud is mostly caused by the existence of a very thin cloud since this type of cloud is usually detected as a clear area using 0.47μm spectral. However, the very thin cirrus is discriminated well using our cloud phase-detection method. The error detection is also caused by the difference in time shift between AHI and Calipso data as well.

We use Eq. 4, Eq.5, and Eq.6 to calculate the cloud altitude ($H$). We used the $T_S$ from local ground temperature measurement in Tokyo, Japan. In the atmospheric window spectral band, we assume that the absorption is almost zero. Hence, the CTT is a BT value using Eq.6. The results of the verification are summarized in Table 2 column #4-7. We classify the ice cloud higher than 6 km and water cloud lower than 6 km. However, sometimes we found a small amount of water cloud at high altitudes. A small amount of ice cloud is also found in the low-level atmosphere. The comparison between the phase-type (column #7) from our method calculation and altitude verification result (column #6) are perfectly matched using our ten datasets. For example, we got an ice cloud over the checking point using dataset #3. Thus, we got 7.2km of cloud altitude from our calculation. So, we confirmed that the altitude verification of dataset #3 is correct. The other nine datasets are verified correctly as well.

Finally, the method has been verified and the result shows a good performance. For further analysis, it needs to be verified using other corrected two-dimensional spatial data, e.g. MODIS standard product. Moreover, it needs to employ another spectral band including the infrared band to enhance the method at the night time.

## 4. CONCLUSIONS

In this study, we carried out cloud detection using a simple algorithm that is essential for rapid processing. We confirm that applying the threshold and simple math operation on pixel-based processing is faster than other algorithms e.g. object-based processing. The method has been described and the verification has been performed using Calipso data showing good results and acceptable for rapid implementation.

## 5. REFERENCES


Bessho K, Date K, Hayashi M, Ikeda A, Imai T, Inoue H, Kumagai Y, Miyakawa T, Murata H, Ohno T, Okuyama A, Oyama R, et al., 2016. An Introduction to Himawari-8/9. J. Meteorol. Soc. Japan 94:151–183.

Chylek P, Robinson S, Dubey MK, King MD, Fu Q, Clodius WB, 2006. Comparison of near-infrared and thermal infrared cloud phase detections. J. Geophys. Res. Atmos. 111:1–8.

Hu Y, 2007. Depolarization ratio–effective lidar ratio relation: Theoretical basis for space lidar cloud phase discrimination. Geophys. Res. Lett. 34:6–9.

Hu Y, Winker D, Vaughan M, Lin B, Omar A, Trepte C, Flittner D, Yang P, Nasiri SL, Baum B, Holz R, Sun W, et al., 2009. CALIPSO/CALIOP cloud phase discrimination algorithm. J. Atmos. Ocean. Technol. 26:2293–2309.

Hu YX, Yang P, Lin B, Gibson G, Hostetler C, 2003. Discriminating between spherical and non-spherical scatterers with lidar using circular polarization: A theoretical study. J. Quant. Spectrosc. Radiat. Transf. 79–80:757–764.

Hummel JR, Kuhn WR, 1981. Comparison of radiative-convective models with constant and pressure-dependent lapse rates. Tellus 33:254–261.

Inoue T, Ackerman SA, 2002. Radiative Effects of Various Cloud Types as Classified by the Split Window Technique over the Eastern Sub-tropical Pacific Derived from Collocated ERBE and AVHRR Data. J. Meteorol. Soc. Japan 80:1383–1394.

Japan Meteorological Agency, 2015. Himawari-8/9 Standard Data User's Guide version 1.2.

Kay JE, Bourdages L, Miller NB, Morrison A, Yettella V, Chepfer H, Eaton B, 2016. Evaluating and improving cloud phase in the Community Atmosphere Model version 5 using spaceborne lidar observations. J. Geophys. Res. 121:4162–4176.

Lutz H-J, Inoue T, Schmetz J, 2003. Notes and Correspondence Comparison of a Split-window and a Multi-spectral Cloud Classification for MODIS Observations. J. Meteorol. Soc. Japan 81:623–631.

Platnick S, Li JY, King MD, Gerber H, Hobbs P V., 2001. A solar reflectance method for retrieving the optical thickness and droplet size of liquid water clouds over snow and ice surfaces. J. Geophys. Res. Atmos. 106:15185–15199.

Purbantoro B, Aminuddin J, Manago N, Toyoshima K, Lagrosas N, Sumantyo JTS, Kuze H, 2019a. Comparison of AquaTerra MODIS and Himawari-8 Satellite Data on Cloud Mask and Cloud Type Classification Using Split Window Algorithm. Remote Sens. 11:2944.

Purbantoro B, Aminuddin J, Manago N, Toyoshima K, Tetuko J, Sumantyo S, Kuze H, 2019b. Evaluation of Cloud Type Classification Based On Split Window Algorithm Using Himawari-8 Satellite Data. IGARSS 2019 - 2019 IEEE Int. Geosci. Remote Sens. Symp. 170–173.

Scorer RS, 1989. Cloud reflectance variations in channel-3. Int. J. Remote Sens. 10:675–686.

Twomey S, Cocks T, 1982. Spectral Reflectance of Clouds in the Near-Infrared: Comparison of Measurements and Calculations. J. Meteorol. Soc. Japan. Ser. II 60:583–592.

Wengang Z, Ming W, Tao Y, Gengke W, Jibao L, Yuqing W, 2010. Study in Retrieval Visibility and Optical Thickness of Fog with MODTRAN. 2010 Int. Conf. Multimed. Technol. 4–6.